TiS Trends in Sciences
TRENDS IN SCIENCES 2027; 24(1): 14059
SPRINT Scholarly Publishing and Repository Integration Center
https://doi.org/10.48048/tis.2027.14059
RESEARCH ARTICLE

Enhanced Mechanical and Bioactive Properties of PVA/CMC/Sericin Hydrogel Facial Masks Containing Pomegranate Extract Fabricated via Freeze–Thaw Technique

Rachata Bunglom[1], Porntipa Pankongadisak[1], Kitipong Kiti[1], Suvimol Surassmo[2] and Orawan Suwantong[1,3,*]

[1]*School of Science, Mae Fah Luang University, Chiang Rai 57100, Thailand*
[2]*National Nanotechnology Center, National Science and Technology Development Agency, Pathum Thani 12120, Thailand*
[3]*Center of Chemical Innovation for Sustainability, Mae Fah Luang University, Chiang Rai 57100, Thailand*

([*]Corresponding author's e-mail: orawan.suw@mfu.ac.th)

Received: 11 April 2026, Revised: 5 June 2026, Accepted: 15 June 2026, Published: 5 September 2026

Abstract

Hydrogel-based facial masks deliver bioactive compounds with favorable skin adhesion and hydration; however, enhancing their mechanical and functional properties remains a challenge. This study developed bioactive polyvinyl alcohol (PVA)/carboxymethyl cellulose (CMC) hydrogels incorporating pomegranate (PG) extract and silk sericin (SS) for cosmetics. The hydrogels were fabricated using a freeze-thaw process (three cycles: −20 °C 20 h; 27 ± 3 °C 4 h). Evaluations included antioxidant and antityrosinase activities, ATR-FTIR, thermal (DSC/TGA), mechanical, adhesion, morphological, *in vitro* release, and cytotoxicity. Stability studies were conducted at 4, 30, and 40 °C for three months. Results demonstrated that PG extract and SS contributed significant antioxidant and antityrosinase activities. ATR-FTIR confirmed molecular interactions within the network. Morphological analysis revealed a dense internal structure that became more compact with SS incorporation. Despite this, all formulations maintained a high water content (~87%), ensuring optimal hydration. The incorporation of SS significantly improved mechanical properties, with compressibility ranging from 43 to 46 N·s and hardness from 104 to 112 N, while maintaining suitable skin adhesion (0.080 - 0.167 kPa). Furthermore, SS effectively modulated the biphasic *in vitro* PG release, with the H-SS5% formulation providing an optimal balance by minimizing the initial burst while sustaining high bioactive delivery. Indirect cytotoxicity evaluation confirmed excellent biocompatibility, with >80% viability in NCTC clone 929 and HDFa cells after 48 h of incubation. The slightly yellow hydrogels were appropriate for cosmetics, and 4 °C storage best preserved visual properties. In conclusion, the developed PVA/CMC hydrogels loaded with PG extract and SS exhibit favorable bioactivity, mechanical performance, safety, and potential applicability as facial masks.

Keywords: Freeze-thaw technique, Polyvinyl alcohol/Carboxymethyl cellulose, Silk sericin, Pomegranate extract, Antioxidant activity, Antityrosinase activity, Hydrogel facial mask

Introduction

The global skincare market was valued at approximately USD 195.8 billion in 2025 and is projected to reach USD 318.1 billion by 2036, indicating sustained expansion driven by increasing consumer demand and ongoing innovation [1]. This sector is the dominant segment of the beauty industry, largely driven by increasing concerns about dermatological conditions such as irritation, hyperpigmentation, excessive sebum production, and premature aging. Consequently, facial masks have emerged as an essential component of daily skincare regimens due to their efficacy in delivering rapid hydration, nourishment, and visible

dermatological improvements [2]. Specifically, hydrogel-based facial masks have gained significant attention owing to their superior water retention capacity and their ability to facilitate the controlled delivery of active ingredients [3,4].

Hydrogels are three-dimensional polymeric networks formed via chemical or physical crosslinking mechanisms, including covalent bonds, ionic interactions, and hydrogen bonding [5]. However, chemically crosslinked systems may reduce the biocompatibility of the material due to residual crosslinking agents [6]. In contrast, physically crosslinked hydrogels, particularly those fabricated via freeze-thaw process, offer a safer and more environmentally friendly alternative. During freeze-thaw process, ice crystal formation induces polymer chain aggregation, while subsequent thawing enables network reorganization, resulting in stable physical crosslinks [7].

Polyvinyl alcohol (PVA) is widely used in hydrogel systems owing to its inherent hydrophilicity, biocompatibility, and excellent film-forming properties [7]. Nevertheless, neat PVA hydrogels often exhibit limited elasticity and suboptimal hydrophilic capacity [8]. To address these limitations, incorporating natural polymers such as carboxymethyl cellulose (CMC), has proven to be an effective strategy. CMC, a biodegradable and biocompatible cellulose derivative, serves to enhance the mechanical strength and thermal stability of PVA-based matrices [9-11]. While PVA/CMC blends are widely reported, leveraging them as a physically crosslinked matrix to stabilize sensitive bioactive compounds remains challenging [12]. In this study, the PVA/CMC blend is strategically selected not merely for structural reinforcement but as an advanced stabilization platform. The dense hydrogen bonding of PVA, combined with the anionic nature of CMC, creates a highly protective microenvironment [13]. This architecture prevents the rapid degradation of sensitive active compounds, effectively overcoming the long-term stability issues common in natural cosmeceutical formulations.

The incorporation of natural bioactive compounds has gained increasing interest in response to consumer demand for safer and more sustainable cosmetic products [14]. Silk sericin (SS), a protein derived from silkworm cocoons, exhibits strong antioxidant activity and has been shown to support cell viability [15-17]. Similarly, pomegranate (PG) extract is rich in polyphenolic compounds with well-documented antioxidant and anti-inflammatory properties [18-20]. Previous studies have demonstrated that PG extract can enhance the functional performance of facial mask materials [21]. However, most existing hydrogel masks incorporate bioactive compounds individually or rely on chemically crosslinked networks, which can raise biocompatibility concerns [22,23]. While SS-based or PG-loaded hydrogels have been studied independently for wound dressing [24-27] or cosmetic [28,29] applications, the simultaneous incorporation of SS and PG extracts into a physically crosslinked PVA/CMC dual-polymeric matrix has not been explored. Therefore, combining SS and PG extract into hydrogel systems offers a promising strategy to enhance its cosmeceutical efficacy.

To address these gaps, this study presents a physically crosslinked PVA/CMC hydrogel system co-loaded with SS and PG extract. Unlike previous studies that focus solely on single-extract systems or chemically crosslinked matrices, this work offers a specific functional advancement by utilizing a solvent-free freeze-thaw method to create a safe, biocompatible matrix capable of delivering dual bioactive benefits. Despite their recognized bioactivities, limited evidence exists regarding the synergistic antityrosinase and antioxidant potential of SS and PG extract within such structurally optimized hydrogel-based delivery systems. This represents a critical gap, as tyrosinase inhibition plays a key role in skin brightening and pigmentation control. Accordingly, this study aims to develop physically crosslinked PVA/CMC/SS hydrogels incorporating PG extract for facial mask applications. The hydrogels were fabricated using the freeze-thaw method, with varying SS concentrations (2.5% (w/w), 5% (w/w), and 10% (w/w) based on the weight of PVA). Antioxidant activity was evaluated using the ABTS assay, while antityrosinase activity was determined via the dopachrome method. The physicochemical properties, including chemical structure, morphology, thermal properties, water content, mechanical properties, adhesiveness, release behaviors, and antityrosinase activity of the released solution were characterized. Furthermore, storage stability was assessed at 4, 30, and 40 °C for 3 months. This was

complemented by thermal cycling stability tests involving five heating-cooling cycles (50 and 4 °C). Both evaluations monitored mechanical properties and color changes using a texture analyzer and UV-visible spectrophotometry. In addition, the indirect cytotoxicity of the hydrogels was investigated to evaluate their biocompatibility and ensure their safety for topical or facial mask applications.

Materials and methods

Materials

Polyvinyl alcohol (PVA 117; MW 100,000 g/mol, viscosity 22 - 30 mPa·s) was purchased from My Skin Recipes (Thailand). Sodium carboxymethyl cellulose (CMC; MW 250,000 g/mol), 2,2'-azino-bis(3-ethylbenzothiazoline-6-sulphonic acid) (ABTS), kojic acid, and L-3,4- dihydroxyphenylalanine (L-DOPA) were purchased from Sigma-Aldrich (USA). *Bombyx mori* silk cocoons were obtained from the Queen Sirikit Sericulture Center (Chiang Mai, Thailand). Pomegranate (PG) extract was purchased from Specialty Natural Product Co., Ltd. (Thailand). All other chemicals and reagents were of analytical grade and used as received.

Silk sericin extraction

Silk sericin (SS) was extracted according to a previously described method [30] with slight modifications. Briefly, Silk cocoons were cut into small pieces, and 5.0 g of the cut cocoons were transferred into a three-neck round-bottom flask. Degumming was carried out by adding 500 mL of 0.5% (w/v) sodium carbonate solution. The mixture was continuously stirred at 85 °C for 45 min. The resulting silk sericin (SS) solution was filtered through filter paper, and the extraction process was repeated twice to maximize SS yield. The combined SS solutions were then lyophilized for 24 h to obtain a light-yellow powder, which was stored in a desiccator prior to further use.

Antioxidant and antityrosinase activities of PG extract and SS

The antioxidant activity of the PG extract and SS was evaluated using the ABTS radical scavenging assay as previously described [31]. The ABTS radical cation was prepared by mixing 7 mM ABTS solution with 2.45 mM potassium persulfate at a volume ratio of 2:1 (v/v). The mixture was incubated in the dark at 4 °C for 16 h. Subsequently, the stock ABTS solution was diluted with deionized (DI) water to achieve a working solution with an absorbance of 0.7 ± 0.02 at 734 nm. Stock SS solutions (6.25 mg/mL) were prepared by dissolving SS in DI water, while the PG extract was used as a concentrated stock solution (100% v/v). The stock solutions were subsequently diluted by serial two-fold dilution using DI water. Aliquots (100 µL) of each diluted sample were added to a 96-well plate, followed by 100 µL of ABTS working solution. Trolox was employed as standard positive control under identical conditions. After incubation for 15 min in the dark, the absorbance was measured at 734 nm using a microplate reader (LTek, Korea). The antioxidant activity was expressed as the half-maximal inhibitory concentration (IC_{50}) and calculated using Eq. (1). To determine the IC_{50} values, the linear regression equations and coefficients of determination (R^2) were derived from the dose-response curves. For instance, the regression equations for the PG extract, SS, and Trolox standard were $y = 100.21x + 8.5757$ ($R^2 = 0.9868$), $y = 138.74x + 2.5264$ ($R^2 = 0.992$), and $y = 5380.8x + 16.585$ ($R^2 = 0.9979$), respectively.

$$\text{Antioxidant activity (\%)} = [(A_{control} - A_{sample})/A_{control}] \times 100 \quad (1)$$

where $A_{control}$ represents the absorbance of the control (without sample) and A_{sample} represents the absorbance of the sample.

The antityrosinase activity of the PG extract and SS was determined using the dopachrome method as previously described [28]. The tyrosinase enzyme was prepared in 0.1 M phosphate buffer solution (pH 6.8), and the L-DOPA substrate was prepared at 15 mM concentration in the phosphate buffer solution. Serial dilutions of the PG extract and SS were transferred into each well of the 96-well plate, followed by the addition of 0.1 M phosphate buffer solution (40 µL), tyrosinase solution (40 µL, 200 units/mL), and L-DOPA substrate (40 µL, 15 mM). The reaction mixture was incubated for 20 min at room temperature, and the absorbance was measured at 490 nm using a microplate reader. The antityrosinase activity was expressed as the IC_{50} value and calculated using Eq. (2):

$$\text{Antityrosinase activity (\%)} = [(A_{control} - A_{sample})/A_{control}] \times 100 \quad (2)$$

where $A_{control}$ represents the absorbance of the control (without sample), and A_{sample} represents the absorbance of the sample.

Preparation of hydrogels containing PG extract

PVA/CMC/SS hydrogels were prepared by first dissolving PVA powder in DI water at 100 °C using a magnetic hotplate stirrer to obtain a 10% (w/v) solution. Subsequently, CMC (1% (w/w), based on PVA weight) was added to the PVA solution and stirred until homogeneous. SS was then incorporated into the PVA/CMC solution at varying concentrations (2.5% (w/w), 5% (w/w), and 10% (w/w), based on PVA weight), followed by continuous stirring at room temperature for 30 min. Thereafter, PG extract (2% (v/v), based on the volume of the PVA solution) was added, and the mixture was stirred until a uniform mixture was formed. This fixed concentration of PG extract was selected based on preliminary *in vitro* bioactivity evaluations (antioxidant and antityrosinase assays) to ensure optimal efficacy, thereby allowing the subsequent evaluations to focus primarily on the effect of the polymer matrix composition. The resulting blends were poured into 6-well plates and subjected to three freeze-thaw cycles. Each cycle consisted of freezing the sample in a laboratory chest freezer at –20 °C for 20 h, followed by thawing at room temperature (27 ± 3 °C) for 4 h. The composition of the resultant hydrogels is summarized in **Table 1**.

Table 1 Compositions of PVA/CMC/SS hydrogels containing PG extract.

Code name	SS concentration (% (w/w) based on PVA solution)	PVA (g)	CMC (g)	PG extract (mL)	SS (mg)	DI water (mL)
H-SS0%	0	1	0.1	0.2	0	10
H-SS2.5%	2.5	1	0.1	0.2	25	10
H-SS5%	5	1	0.1	0.2	50	10
H-SS10%	10	1	0.1	0.2	100	10

Chemical and morphological characterization

Attenuated total reflectance Fourier-transform infrared (ATR-FTIR) analysis

The chemical structures of SS, PG extract, CMC, PVA, and hydrogels (H-SS0%, H-SS2.5%, H-SS5%, and H-SS10%) were characterized using an ATR-FTIR spectrophotometer (Thermo Fisher Scientific, USA). The spectra were recorded in the wavenumber range of 4,000 - 500 cm^{-1} at a resolution of 16 cm^{-1} in transmittance mode.

Morphological analysis by Scanning Electron Microscopy (SEM)

The surface and cross-sectional morphologies of the freeze-thawed hydrogels were investigated using a field emission scanning electron microscope (FE-SEM, TESCAN MIRA, Czech Republic). Prior to the observation, the fully swollen hydrogel samples were lyophilized using an Alpha 3-4 LSCbasic freeze dryer (Martin Christ, Germany) for 24 h to preserve their internal porous structures. For cross-sectional analysis, the freeze-dried hydrogels were carefully fractured using liquid nitrogen. The dried specimens were then fixed onto aluminum stubs using double-sided conductive carbon tape and sputter-coated with a thin layer of gold for 60 s under vacuum using a Quorum Q150R S sputter coater to prevent charging effects. The SEM micrographs were captured at an accelerating voltage of 15 kV at 500x magnification.

Thermal properties

Thermogravimetric analysis (TGA)

The thermal degradation behavior of hydrogels (H-SS0%, H-SS2.5%, H-SS5%, and H-SS10%) was analyzed using TGA (TGA/DSC3+ HT, METTLER TOLEDO, Switzerland). Dried samples (5 - 10 mg) were placed in alumina crucibles and heated from 25 to 700 °C at a heating rate of 10 °C/min under a nitrogen atmosphere.

Differential scanning calorimetry (DSC)

The thermal properties of hydrogels (H-SS0%, H-SS2.5%, H-SS5%, and H-SS10%) were analyzed using DSC (DSC3+, METTLER TOLEDO, Switzerland) equipped with a liquid nitrogen cooling system. Dried samples (5 - 8 mg) were sealed in aluminum pans and heated from 25 to 700 °C at a heating rate of 10 °C/min under a nitrogen atmosphere with a gas flow rate of 40 mL/min.

Physical and mechanical properties

Color measurement of hydrogels

The colorimetric properties of hydrogels (H-SS0%, H-SS2.5%, H-SS5%, and H-SS10%) were analyzed using a UV-Vis spectrophotometer (Lambda 850+, PerkinElmer, USA). Measurements were performed under the CIE standard illuminant C. Color parameters were expressed in the CIE $L^*a^*b^*$ color space, where L^* represents lightness (0 = black to 100 = white), a^* indicates the red-green axis (positive = red and negative = green), and b^* represents the yellow-blue axis (positive = yellow and negative = blue).

Water content of hydrogels

The water content of the freeze-thawed hydrogels was determined using a gravimetric method. Briefly, the freshly prepared hydrogel samples with a diameter of 1.5 cm were accurately weighed to record their initial wet weights (W_i). The samples were then lyophilized using a freeze-dryer. The final dry weights (W_d) were then recorded. The water content percentage of the hydrogels was calculated using Eq. (3):

$$\text{Water content (\%)} = [(W_i - W_d)/ W_i] \times 100 \quad (3)$$

All measurements were performed in triplicate, and the results were reported as mean ± standard deviation (SD).

Mechanical properties of hydrogels

The mechanical properties of hydrogels (H-SS0%, H-SS2.5%, H-SS5%, and H-SS10%) were evaluated using texture profile analysis (TPA). Measurements were performed using a texture analyzer (Stable Micro Systems Ltd., UK) equipped with a cylindrical probe (P/0.5R). The analysis was conducted at a compression strain of 80% with a crosshead speed of 5 mm/s. Hardness was defined as the maximum force (N) recorded during the first compression cycle. Compressibility was calculated as the work required to deform the sample, represented by the area under the force-time curve during the first compression cycle.

Adhesiveness of hydrogels

The adhesive properties of hydrogels (H-SS0%, H-SS2.5%, H-SS5%, and H-SS10%) were evaluated using a texture analyzer in adhesion test mode. Porcine skin samples (1×1 cm) were mounted on the upper surface of a cylindrical probe (P/0.5P). The probe-mounted porcine skin was brought into contact with the hydrogel surface under a constant force of 0.02 N for 30 s. The probe was then withdrawn at a speed of 2 mm/s. Adhesive strength was determined as the maximum detachment force (N) required to separate the porcine skin from the hydrogel surface.

In vitro release study

The release profiles of PG extract from the hydrogels were investigated using the total immersion method. PVA/CMC/SS hydrogels containing PG extract were cut into circular discs (10 mm in diameter). A pre-weighed hydrogel sample was immersed in a 50-mL centrifuge tube containing 13 mL of phosphate-buffered saline (pH 5.5) as the release medium. The tubes were placed in an incubator shaker (Model ES-60+, MIULAB, China) maintained at 32 °C for skin application with a constant shaking speed of 100 rpm. At predetermined time intervals (e.g., 15, 30, 45, and 60 min), an aliquot of 1 mL was withdrawn from the release medium. To maintain sink conditions, an equal volume of fresh medium at the same temperature was immediately added back to the system. The concentration of the released active substance was quantified using a UV-Vis spectrophotometer (Lambda 850+, PerkinElmer, USA) at a wavelength of 269 nm. The cumulative release percentage was calculated using a standard calibration curve for the PG extract.

Antityrosinase activity of the released solution

PVA/CMC/SS hydrogels containing PG extract were cut into circular discs (10 mm in diameter) and immersed in 13 mL of phosphate-buffered saline (pH 5.5) at 32 °C for 15 min. The released solution was collected and analyzed for antityrosinase activity using

the dopachrome method. An aliquot of the released solution (80 µL) was mixed with phosphate buffer solution (0.1 M, pH 6.8), tyrosinase solution (40 µL), and L-DOPA substrate (40 µL). After incubation, the absorbance was measured at 490 nm using a microplate reader. The percentage of antityrosinase activity was calculated using Eq. (2).

In vitro cytotoxicity assay

The *in vitro* cytotoxicity of the hydrogels was evaluated following the ISO 10993-5 guidelines using the MTT assay. Mouse fibroblasts (NCTC clone 929) and adult human dermal fibroblasts (HDFa) were separately seeded in a 96-well tissue culture plate at a density of 1×10^4 cells/well in Dulbecco's Modified Eagle Medium (DMEM; Gibco, USA) supplemented with 10% fetal bovine serum (Gibco, USA) and 1% antibiotic-antimycotic formulation (Gibco, USA). The cells were incubated for 24 h at 37 °C in a humidified atmosphere containing 5% CO_2. Prior to testing, the hydrogel samples were sterilized under ultraviolet (UV) light for 30 min per side. To prepare the sample extracts, the sterilized hydrogels were immersed in the culture medium at a concentration of 100 mg/mL and incubated for 24 h at 37 °C. This extraction medium was then diluted with fresh culture medium to produce a concentration series of 5, 10, 25, 50, and 100 mg/mL. The initial culture medium in the 96-well plate was discarded and replaced with 100 µL of the prepared hydrogel extracts. The cells were then incubated for predetermined periods (i.e., 1, 24, and 48 h). Cells cultured in standard medium without any extract served as the negative control.

After the predetermined incubation periods, the extract solutions were removed, and MTT solution (5 mg/mL in PBS) was added to each well, followed by incubation for 3 h in the dark. The formazan crystals formed by viable cells were dissolved in 100 µL of dimethyl sulfoxide (DMSO). The absorbance was measured at 570 nm using a microplate spectrophotometer (Model INNO, LTek, South Korea). The relative cell viability was calculated as a percentage relative to the negative control using Eq. (4).

$$\text{Cell viability (\%)} = (A_{sample}/A_{control}) \times 100 \quad (4)$$

where A_{sample} represents the absorbance of the cells treated with the hydrogel extract, and $A_{control}$ represents the absorbance of the cells treated with the standard culture medium (negative control).

Stability test of hydrogels

The stability of hydrogels (H-SS0%, H-SS2.5%, H-SS5%, and H-SS10%) was evaluated under different storage conditions. Samples were stored in sealed, light-protected polyethylene bags at 4, 30, and 40 °C for up to 3 months. Evaluations were conducted at 1, 2, and 3 months. Thermal cycling stability was assessed by subjecting the hydrogels to 7 heating-cooling (H/C) cycles. Each cycle consisted of heating at 50 °C in a hot air oven for 24 h and cooling at 4 °C in a laboratory chest freezer for 24 h. Stability was assessed by monitoring changes in visual appearance, mechanical properties, and color. Mechanical and color properties were evaluated using the methods described above.

Statistical analysis

The experimental results were reported as mean values ± standard deviation (SD). Statistical analysis was performed using one-way analysis of variance (ANOVA), followed by Tukey's post hoc test, using IBM SPSS (USA). Differences between treatment groups were considered statistically significant at $p < 0.05$.

Results and discussion

Antioxidant and antityrosinase activities of PG extract and SS

The antioxidant and antityrosinase activities of PG extract and SS were evaluated using the ABTS radical scavenging assay and the dopachrome method, respectively. The antioxidant activity, expressed as IC_{50} values, was 0.458% (v/v) for PG extract and 0.337 mg/mL for SS. For comparison, the standard antioxidant Trolox was also evaluated, yielding the IC_{50} value of 0.0062 mg/mL. Comparing our extracts to this reference standard indicates that, while their activities are naturally lower than a pure compound, both PG extract and SS exhibit relevant radical scavenging capacities suitable for topical formulations and cosmeceutical products. For antityrosinase activity, PG extract exhibited the IC_{50} value of 52.57% (v/v), while SS showed an IC_{50} value of 7.19 mg/mL. According to

previous studies, the bioactivity of PG extract is often attributed to its high content of polyphenolic constituents, particularly ellagic acid and punicalagin [19,20]. These compounds have been reported by other researchers to exhibit potent radical-scavenging capacity and are reported to inhibit tyrosinase activity through interactions with the enzyme active site, including copper ion chelation [32]. Furthermore, their antioxidant function is generally associated with efficient electron- and hydrogen-donating abilities, enabling effective neutralization of reactive oxygen species [19,32]. Therefore, the activities observed in our PG extract might be explained by the presence of similar bioactive compounds. Regarding SS, literature suggests that silk sericin contains various amino acids and peptides [15], including serine, and that these components may contribute to its antioxidant activity through radical scavenging and metal-chelating mechanisms [16,25]. Additionally, SS has been reported to exhibit tyrosinase inhibitory activity, potentially due to its ability to interact with the enzyme and reduce substrate oxidation [33]. These results indicate that both PG extract and SS exhibit bioactive properties relevant to antioxidant and antityrosinase functions, suggesting their potential application in cosmetic and biomaterial systems. However, further compositional analysis and mechanistic studies are required to fully elucidate the specific active compounds and their precise mechanisms in these specific extracts.

ATR-FTIR analysis of hydrogels

The chemical compositions and molecular interactions within the hydrogels were characterized using ATR-FTIR spectroscopy. **Figure 1** presents the spectra of the individual components (PG extract, SS, CMC, and PVA) and the fabricated hydrogels (H-SS0% and H-SS10%). The spectrum of CMC showed distinct peaks at 1,597 and 1,419 cm^{-1}, corresponding to asymmetric and symmetric stretching of carboxylate ($–COO^–$) groups, as well as a peak at 1,059 cm^{-1} associated with C–O stretching [10]. PVA exhibited a broad absorption band around 3,309 cm^{-1}, corresponding to O–H stretching vibrations, along with characteristic peaks at 1,425 and 1,095 cm^{-1}, attributed to C–H bending and C–O stretching vibrations, respectively [7]. The PG extract displayed prominent absorption bands at 3,375 and 1,654 cm^{-1}, corresponding to O–H stretching and C=O vibrations of polyphenolic compounds, as well as a peak at 1,456 cm^{-1} related to the aromatic ring vibrations [19]. SS exhibited characteristic peaks at 1,654 cm^{-1} (amide I) and 1543 cm^{-1} (amide II), indicating the presence of protein structures [34]. In the spectra of H-SS0% and H-SS10% hydrogels, the shifting of PVA's characteristic peaks from 1,425 and 1,095 cm^{-1} to 1,415 and 1,088 cm^{-1}, respectively, confirms the incorporation of CMC within the PVA matrix. This shift suggests the formation of intermolecular interactions, primarily hydrogen bonding, between PVA and CMC chains [35]. For the H-SS10% hydrogel, the appearance of a peak at 1,654 cm^{-1}, which overlaps with the amide I band of SS and the carbonyl stretching of the PG extract, further confirms the successful entrapment and uniform distribution of SS within the hydrogel network [36]. These results indicate that the freeze-thaw process promoted the formation of physically crosslinked hydrogels through hydrogen bonding and the development of PVA microcrystalline domains, resulting in a stable three-dimensional network without the use of chemical crosslinking agents [6].

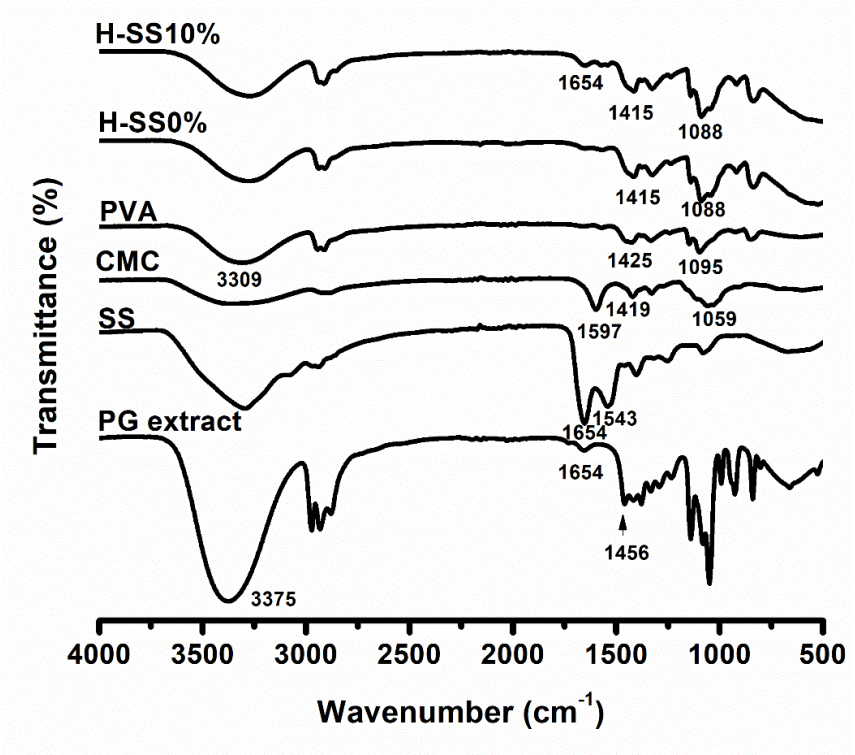

Figure 1 ATR-FTIR spectra of PG extract, SS, CMC, PVA, H-SS0%, and H-SS10%.

SEM morphological analysis of hydrogels

The cross-sectional morphology of the hydrogels was examined using SEM, as shown in **Figure 2**. All samples exhibited a highly folded, continuous, and compact internal structure, typical of hydrogels lacking apparent macroscopic pores. The H-SS0% exhibited a generally smooth morphology interspersed with subtle wrinkles. However, the incorporation of SS significantly altered the internal morphology. As the SS concentration increased from 2.5% to 10%, the internal structure became progressively rougher, denser, and more tightly packed. Notably, the H-SS10% exhibited the most compact and agglomerated morphology, characterized by thick and highly condensed polymer folds.

The dense and highly wrinkled morphology observed across all hydrogels is a direct consequence of the mixing and freeze-thawing process used for hydrogel fabrication. During the freezing phase, the formation of ice crystals forces the PVA and CMC polymer chains to phase-separate and aggregate, creating physical crosslinking points (crystallites) that form a tightly packed network upon thawing [37]. The progressive increase in structural density with higher SS concentrations can be explained by extensive intermolecular interactions. SS is rich in polar functional groups, particularly amino and hydroxyl groups, which facilitate robust hydrogen bonding with both the PVA/CMC polymer chains and the incorporated PG [38]. These strong interactions act as additional physical crosslinking junctions, pulling the polymer network closer together and resulting in the thicker, more rigid, and highly compacted structure observed in the SEM images of H-SS5% and H-SS10%.

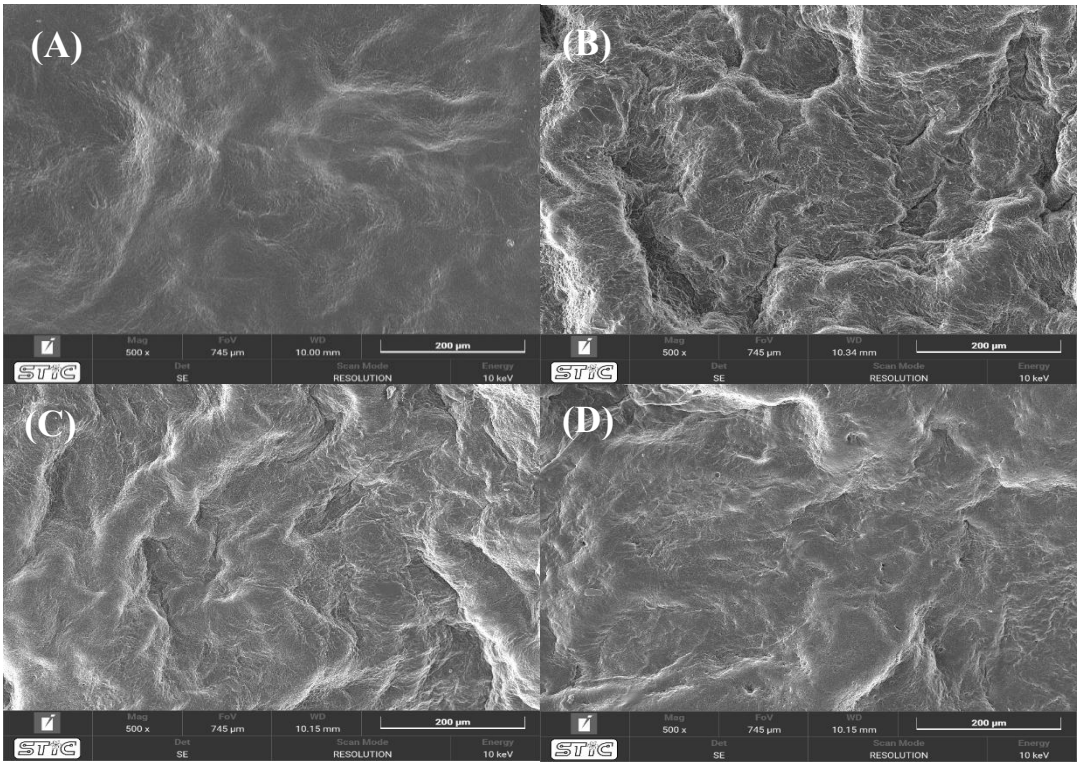

Figure 2 Cross-sectional SEM images of (A) H-SS0%, (B) H-SS2.5%, (C) H-SS5%, and (D) H-SS10%. Images were taken at a magnification of 500x with a scale bar of 200 µm.

Thermogravimetric analysis (TGA) of hydrogels

TGA and DTG analysis revealed a four-stage thermal degradation behavior of the hydrogels, as shown in **Figure 3** and the Supplementary Material. The thermograms of PVA/CMC/SS hydrogels containing PG extract (H-SS0%, H-SS2.5%, H-SS5%, and H-SS10%) exhibited complex weight loss profiles. The initial stage, occurring between 30 and 150 °C (with a DTG peak around 90 - 138 °C), is attributed to the evaporation of physically bound and free water within the hydrogel matrix, reflecting its hydrophilic nature [39]. The second stage, observed in the range of 200 - 260 °C (DTG peak at ~230 °C), corresponds to the initial degradation of side groups, such as the dehydration of PVA and the decomposition of heat-sensitive components from the PG extract and SS [7,34]. The third stage, occurring between 260 and 380 °C (with a prominent DTG peak around 300 °C), represents the main thermal degradation of the polymer backbone [39]. This stage involves the decarboxylation of CMC, the scission of the PVA hydrocarbon chain, and the breakdown of protein structures in SS. The fourth stage, observed from 380 to 550 °C (DTG peak at ~410 - 440 °C), is associated with the further degradation of residual organic fragments and carbonized structures [39]. Above 600 °C, the mass loss stabilized, resulting in a residual mass corresponding to char formation. Interestingly, a slight decrease in final residual weight was observed with increasing SS content, which might be due to the relatively lower thermal stability and higher volatility of protein fragments at extreme temperatures. Notably, the incorporation of SS led to a slightly more pronounced second degradation stage, indicating that the protein components initiate thermal decomposition earlier than the synthetic polymer matrix. However, the overall degradation profiles remained highly similar across all formulations, suggesting that SS incorporation does not significantly compromise the overall thermal stability of the hydrogel system [34,40].

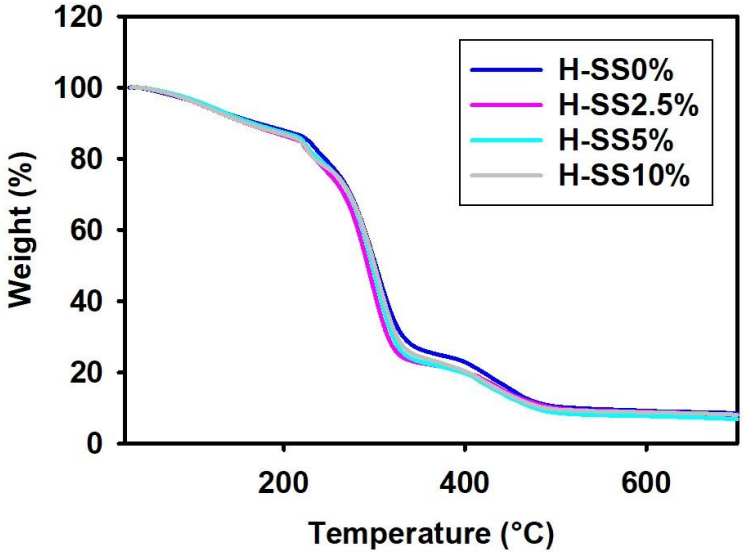

Figure 3 TGA thermograms of H-SS0%, H-SS2.5%, H-SS5%, and H-SS10%.

Differential scanning calorimetry (DSC) analysis of hydrogels

The DSC thermograms of CMC/PVA/SS hydrogels containing PG extract are presented in **Figure 4**. All hydrogel formulations exhibited a broad endothermic region below 150 °C, attributed to the evaporation of free and bound water within the hydrogel matrix, which strongly supports the initial weight loss stage observed in the TGA results. A prominent endothermic peak was observed in the temperature range of approximately 220 - 330 °C for all samples, corresponding to thermal transitions associated with polymer structural changes and degradation of the polymer network. Interestingly, this main endothermic peak exhibited a progressive shift toward higher temperatures with increasing incorporation of SS. While the peak for H-SS0% appeared near 295 °C, it shifted to approximately 301 °C for H-SS5%, and reached a maximum of approximately 312 °C for the H-SS10% hydrogel. Notably, the H-SS10% hydrogel exhibited a more pronounced and shifted endothermic peak, suggesting that a higher concentration of SS (10%) promotes stronger intermolecular interactions within the polymer matrix, likely due to the formation of a more robust hydrogen-bonded network between PVA, CMC, and SS. At higher temperatures (above 400 °C), the thermograms showed gradual thermal degradation behavior, consistent with the decomposition of polymeric and bioactive components [39]. Overall, the DSC results suggest that the incorporation of SS, particularly at 10%, significantly enhances the molecular interactions, thereby improving the thermal resistance of the hydrogel network [40]. These thermodynamic findings complement the TGA profiles, providing a deeper understanding of how the internal polymeric interactions influence the overall thermal behavior of the hydrogels.

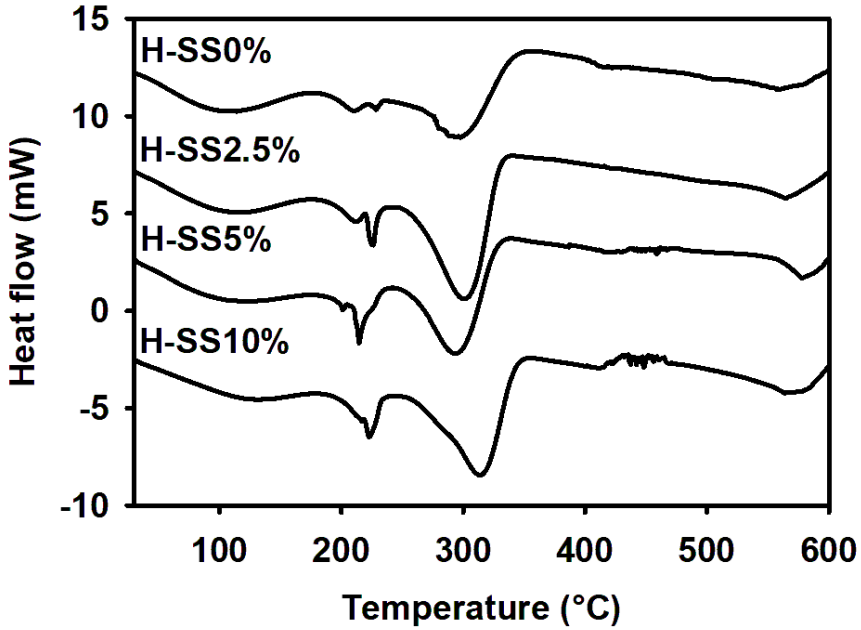

Figure 4 DSC thermograms of H-SS0%, H-SS2.5%, H-SS5%, and H-SS10%.

Color measurement of hydrogels

The colorimetric properties of the hydrogels were evaluated using the CIE *L*a*b** color space system (**Figure 5**). The *L** values ranged from 75.94 to 84.37, indicating a relatively light appearance. However, a progressive decrease in *L** was observed with increasing SS content, suggesting that the hydrogels became slightly darker. The *a** values were negative for all formulations, indicating a shift toward green tones. The magnitude of negative *a** values increased with the addition of SS, showing a more pronounced green coloration at higher SS levels. However, at 10% SS, a slight reduction in green tone was observed, which may be attributed to the inherent yellow coloration of SS. The *b** values increased from negative to positive values with the addition of SS, indicating a transition from slightly bluish tones (H-SS0%) to more pronounced yellow coloration at higher SS levels. These color changes can be attributed to the presence of PG extract, which contains polyphenolic compounds such as ellagic acid and punicalagin. These compounds exhibit natural yellow to brown coloration and are susceptible to oxidation, leading to the formation of quinone-like structures that contribute to increased yellowness. In addition, interactions between polyphenols and the polymer matrix may influence their distribution and optical properties. Mild oxidation during processing or storage may further contribute to the observed color shift. Overall, the hydrogels maintained a relatively light and uniform appearance despite compositional variations. These results suggest that the addition of SS influences the color characteristics of the system without significantly compromising visual uniformity.

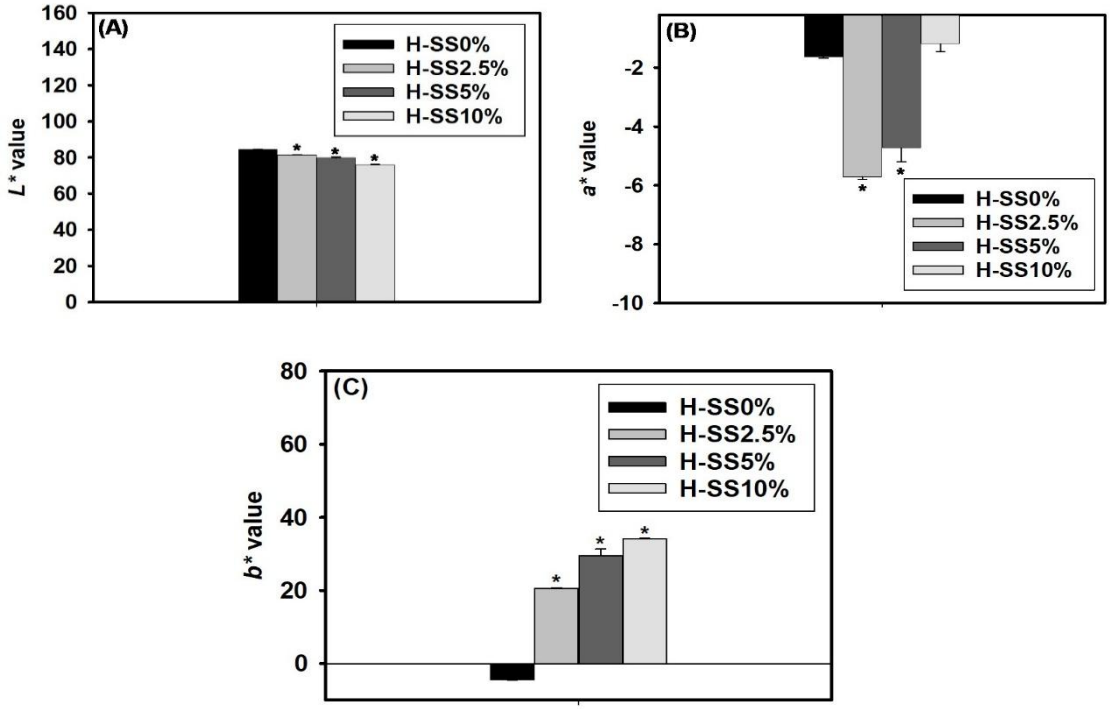

Figure 5 (A) L^*, (B) a^*, and (C) b^* values of PVA/CMC/SS hydrogels containing PG extract. $^*p < 0.05$ compared with H-SS0%. Data are expressed as mean ± SD (n = 3).

Water content of hydrogels

As shown in **Table 2**, all hydrogels exhibited high water retention capacity, ranging from 87.11% to 87.71%, confirming the strong hydrophilicity of the polymer matrix. The incorporation of SS at various concentrations resulted in only minor fluctuations in water content, suggesting that the hydrogel network maintains a stable and highly hydrated equilibrium state. Overall, the addition of SS did not compromise the excellent moisture-retaining capacity of the network. In cosmetic applications, facial masks must balance high hydration efficacy with mechanical durability. These formulations, with approximately 87% water content, provide an optimal balance between deep moisture delivery and structural integrity [41]. Compared with conventional non-woven masks, this high water content may provide a more occlusive interface, thereby reducing transepidermal water loss and supporting sustained hydration of the stratum corneum [42]. Furthermore, the observed water retention range ensures the essential physical stability required for manufacturing, packaging, and handling. Consequently, the H-SS hydrogels demonstrate great promise for advanced cosmetic facial mask applications.

Mechanical properties and adhesiveness of hydrogels

The mechanical properties of H-SS0%, H-SS2.5%, H-SS5%, and H-SS10% are summarized in **Table 2**. While a universal testing machine (UTM) is conventionally used to determine fundamental stress-strain parameters at material failure, texture analysis was strategically selected for this study. Although it is an empirical method, it better simulates the practical handling and sensory characteristics required for a cosmeceutical facial mask, allowing for the direct evaluation of critical consumer-use parameters: Compressibility, hardness, and adhesiveness. As observed, the compressibility values were approximately 43, 45, 46, and 44 N·s, respectively, while the hardness values were approximately 104, 108, 112, and 108 N, respectively. Both compressibility and hardness increased with increasing SS content up to 5%, followed by a slight decrease at 10% SS. This trend suggests that moderate SS incorporation enhances the mechanical strength of the hydrogel by improving intermolecular interactions within the polymer network [43]. However, at higher SS content (H-SS10%), a slight reduction in mechanical properties was observed,

possibly due to disruption of the optimal polymer network interactions [44]. In contrast, the adhesiveness values were approximately 0.080, 0.078, 0.082, and 0.167 kPa for H-SS0%, H-SS2.5%, H-SS5%, and H-SS10%, respectively, showing a significant increase at 10% SS. This enhancement in adhesiveness may be attributed to the presence of polar amino acids in SS, such as serine and aspartic acid, which can promote hydrogen bonding and electrostatic interactions with the skin surface [45]. Overall, these results indicate that SS plays an important role in modulating both the mechanical and adhesive properties of the hydrogels, with 5% SS providing optimal mechanical performance and 10% SS enhancing adhesive behavior.

Table 2 Water content, compressibility, hardness, and adhesiveness of PVA/CMC/SS hydrogels containing PG extract (n = 3).

Sample	Water content (%)	Compressibility (N·s)	Hardness (N)	Adhesiveness (kPa)
H-SS0%	87.61 ± 0.03	43.18 ± 2.36	104.38 ± 3.52	0.080 ± 0.026
H-SS2.5%	87.71 ± 0.03*	44.97 ± 2.18	108.28 ± 3.61	0.078 ± 0.010
H-SS5%	87.61 ± 0.01	46.26 ± 1.45	112.21 ± 1.97	0.082 ± 0.011
H-SS10%	87.11 ± 0.01*	44.16 ± 1.72	108.49 ± 3.31	0.167 ± 0.002*

*$p < 0.05$ compared with H-SS0%.

In vitro release study of PG extract from hydrogels

The *in vitro* PG release profiles (**Figure 6**) showed a biphasic pattern in all hydrogels, characterized by an initial 15-min burst followed by sustained release. H-SS0% displayed the highest initial burst, releasing 47.8% of PG within the first 15 min and reaching 78.4% at 60 min. The incorporation of SS progressively suppressed this early burst; at 15 min, the cumulative release decreased to 42.8% for H-SS2.5% and 21.8% for H-SS5%. Notably, H-SS5% had the lowest initial release, which was significantly lower than that of H-SS0% ($p < 0.05$). However, H-SS5% maintained a steady output, ultimately reaching 78.2% at 60 min, a value comparable to H-SS0%. In contrast, the highest SS concentration (H-SS10%) restricted PG release throughout the test, leveling off at 72.4% by 60 min. The initial burst release across all samples is primarily attributed to the rapid dissolution and outward diffusion of PG molecules situated near the hydrogel surface. Once these surface molecules are depleted, the release is controlled by the slower diffusion of PG molecules entrapped deeper within the polymeric matrix. This restricted release in high-SS hydrogels is closely tied to the dense network formed during the freeze-thaw process. Adding SS to the PVA/CMC matrix increases the physical crosslinking density [46]. Furthermore, the abundant polar amino and hydroxyl groups in SS facilitate robust hydrogen bonding with both the PVA/CMC backbone and the polyphenolic compounds in the PG extract [47]. These strong interactions yield a more compact polymer network, which limits hydrogel swelling and polymer chain mobility. Consequently, diffusion resistance increases, hindering the escape of PG molecules. As supported by the SEM findings, this highly condensed network physically restricts water penetration and reduces the free volume available for chain relaxation, thereby imposing a significant barrier to diffusion [48]. Overall, the H-SS5% formulation provides the most optimal balance, successfully minimizing the early burst effect while sustaining a high bioactive release profile.

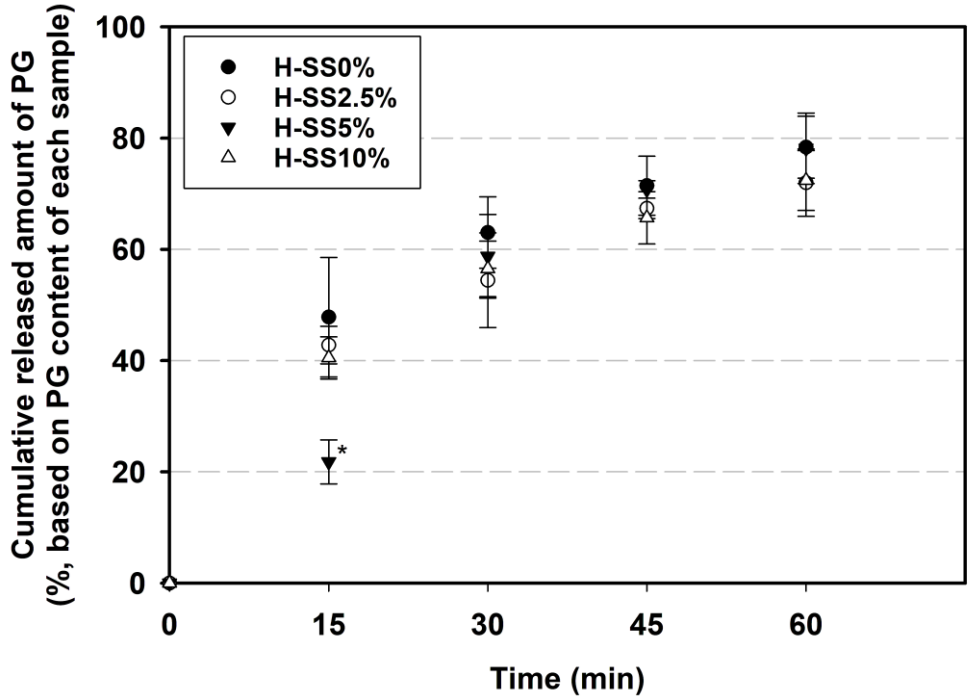

Figure 6 *In vitro* cumulative release profiles of PG extract from the hydrogels. * $p < 0.05$ compared with the H-SS0%. Data are expressed as mean ± SD (n = 3).

Antityrosinase activity of released solution from hydrogels

The tyrosinase inhibitory activity of the released solutions from the hydrogels is presented in **Figure 7**. Statistical analysis revealed that the antityrosinase activity was significantly influenced by the SS concentration. The control sample (H-SS0%) exhibited the lowest inhibitory activity at 4.8% (denoted by letter (a)). Incorporation of 2.5% SS (H-SS2.5%) significantly enhanced the inhibition to 15.4% ((b)), which further increased to a maximum of 31.3% in H-SS5% ((c)), representing a statistically significant stepwise improvement ($p < 0.05$). However, increasing the SS concentration further to 10% (H-SS10%) resulted in a plateau (30.9%), sharing the same letter ((c)) with H-SS5%. This explicitly confirms that there is no statistically significant difference between H-SS5% and H-SS10% ($p > 0.05$). The released solutions exhibited measurable antityrosinase activity, which can be attributed to the presence of polyphenolic compounds in the PG extract [32], known to inhibit tyrosinase activity. In addition, SS may contribute to this effect through its antioxidant properties and potential interactions with the enzyme. The increase in inhibitory activity with SS addition may be associated with improved retention and release of bioactive compounds within the hydrogel matrix. However, the comparable activity observed at higher SS content suggests that further increases in SS concentration do not significantly enhance antityrosinase activity. Overall, these results indicate that the addition of SS influences the antityrosinase activity of the released solutions, with optimal performance observed at 5% SS.

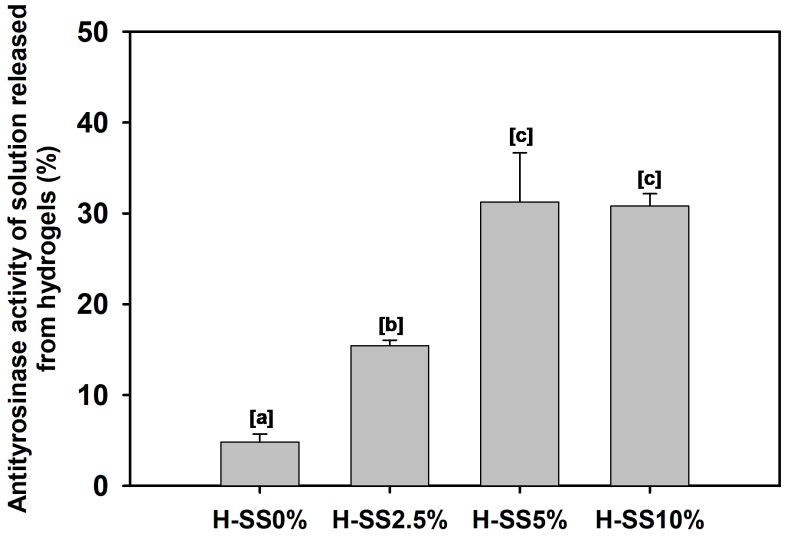

Figure 7 Antityrosinase activity of the solution released from PVA/CMC/SS hydrogels containing PG extract after 15 min of immersion in PBS (pH 5.5 at 32 °C). Different lowercase letters above the bars indicate statistically significant differences between groups ($p < 0.05$). Data are expressed as mean ± SD (n = 3).

***In vitro* cytotoxicity of hydrogels**

The indirect cytotoxicity of the hydrogels (H-SS0%, H-SS2.5%, H-SS5%, and H-SS10%) was evaluated using NCTC clone 929 and HDFa cells over incubation periods of 1, 24, and 48 h. As shown in **Figure 8**, across all tested extract concentrations (5 - 100 mg/mL) and time intervals, cell viability for both cell lines remained exceptionally high, consistently exceeding 80%. Although most hydrogel extract groups exhibited a statistically significant decrease in cell viability compared with the untreated control, the reduction was marginal. A slight, dose-dependent attenuation in cell viability was noted at elevated extract concentrations (50 and 100 mg/mL). Furthermore, prolonged exposure up to 48 h (**Figures 8(E)** and **8(F)**) did not result in a substantial decline in cell survival when compared to the 1 h (**Figures 8(A)** and **8(B)**) and 24 h (**Figures 8(C)** and **8(D)**) time points. Notably, incorporation of the SS component at 10% (H-SS10%) did not induce severe cytotoxicity compared to the hydrogel (H-SS0%), indicating that the active additive is well tolerated by the cellular models within the evaluated parameters.

These findings substantiate the excellent *in vitro* biocompatibility of these hydrogels. According to ISO 10993-5, the standard for biological evaluation of materials, a substance is generally classified as cytotoxic if cell viability falls below 70% of the control [49]. This dual evaluation, using both NCTC clone 929 (a standard continuous cell line for preliminary cytotoxicity screening) and HDFa (primary human dermal fibroblasts), provides a robust safety profile. Specifically, the sustained viability of human-derived HDFa cells over 48 h is particularly relevant for dermatological formulations, demonstrating that these hydrogels are non-cytotoxic and highly suitable for cosmetic applications, specifically as biocompatible facial masks for prolonged skin contact.

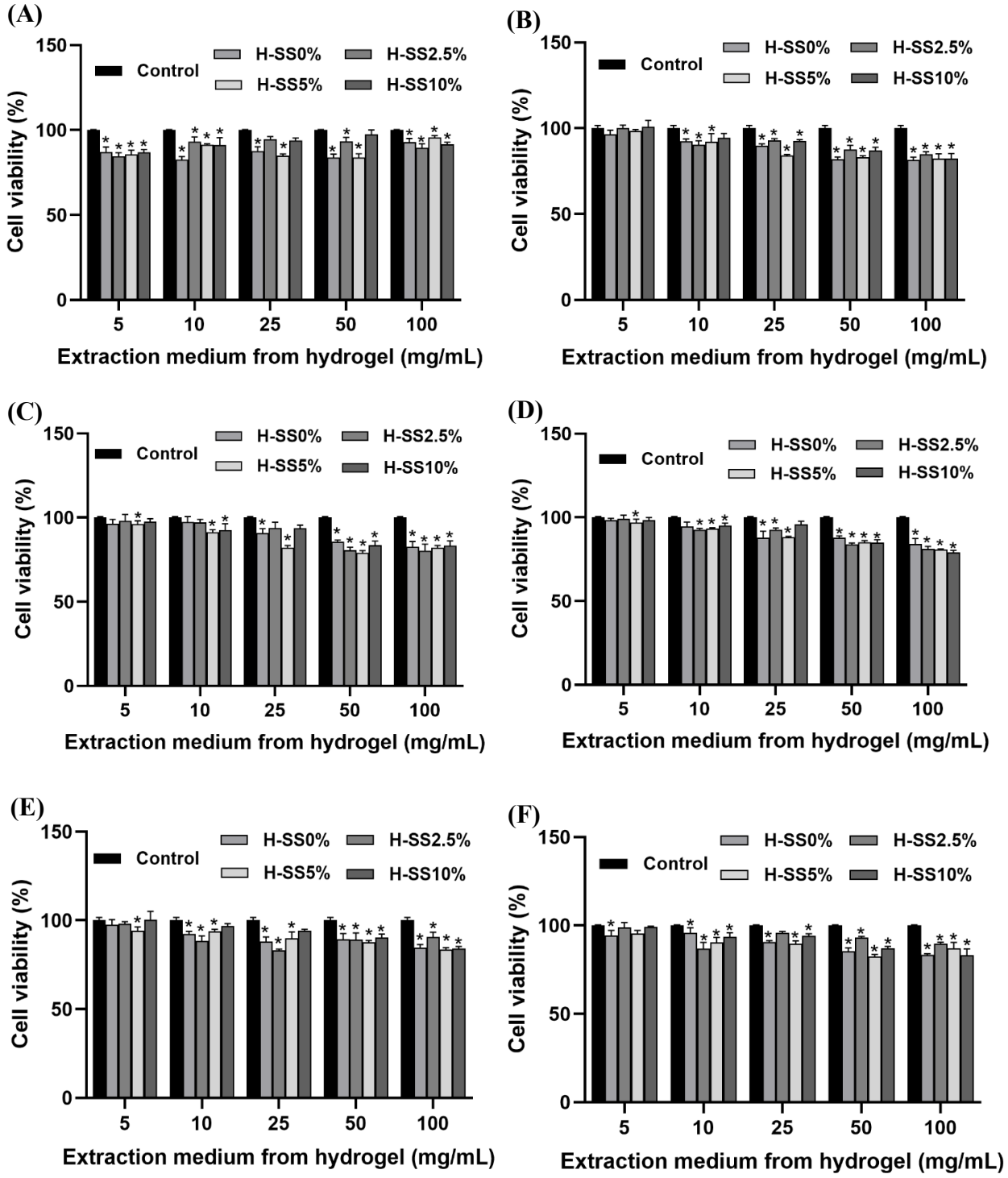

Figure 8 Indirect cytotoxicity evaluation of NCTC clone 929 and HDFa cells treated with hydrogel extracts at different time points. Cell viability of NCTC clone 929 cells is presented at (A) 1 h, (C) 24 h, and (E) 48 h, while HDFa at (B) 1 h, (D) 24 h, and (F) 48 h. * $p < 0.05$ compared with the control. Data are expressed as mean ± SD (n = 3).

Stability test of hydrogels

Color stability

The color stability of the hydrogels stored at 4, 30, and 40 °C over 1 - 3 months, together with those subjected to heating-cooling (H/C) cycles, is presented in **Figures 9 - 12**. Representative photographs of the hydrogels under each storage condition are shown in **Figure 13** and the Supplementary Material, illustrating the corresponding visual color changes. At 4 °C, the hydrogels showed minimal changes in *L**, *a**, and *b** values over time, indicating good color stability under refrigerated conditions. At elevated temperatures (30 and 40 °C), slight variations in *L** were observed, while the *a** values remained negative but showed increased fluctuations. The *b** values generally increased during storage, indicating enhanced yellow coloration, which may be associated with temperature-dependent changes in polyphenolic compounds. As reported in previous studies, elevated temperatures favor the oxidation and polymerization of polyphenols (such as flavanols) from PG, leading to the formation of yellow-brown pigments [50]. Under H/C cycles, more pronounced changes were observed. The *L** values decreased, indicating a darker and more opaque appearance. This phenomenon is strongly associated with the structural rearrangement of the polymer matrix induced by repeated thermal cycling. The fluctuating temperatures promote phase separation and the formation of robust inter- and intramolecular hydrogen bonds, leading to increased micro-crystallization and matrix densification [51,52]. Consequently, the denser polymer network enhances light scattering and reduces light transmission, effectively lowering the *L** value [37]. Simultaneously, the *b** values showed a reduction, suggesting a decrease in yellow intensity. The *a** values remained negative with minor variations. Overall, the hydrogels exhibited temperature-dependent changes in color parameters. The highest stability was observed at 4 °C, moderate changes occurred at 30 and 40 °C, and the highest variation was observed under thermal cycling conditions. These changes are likely related to structural rearrangement of the polymer network and alterations in polyphenolic components.

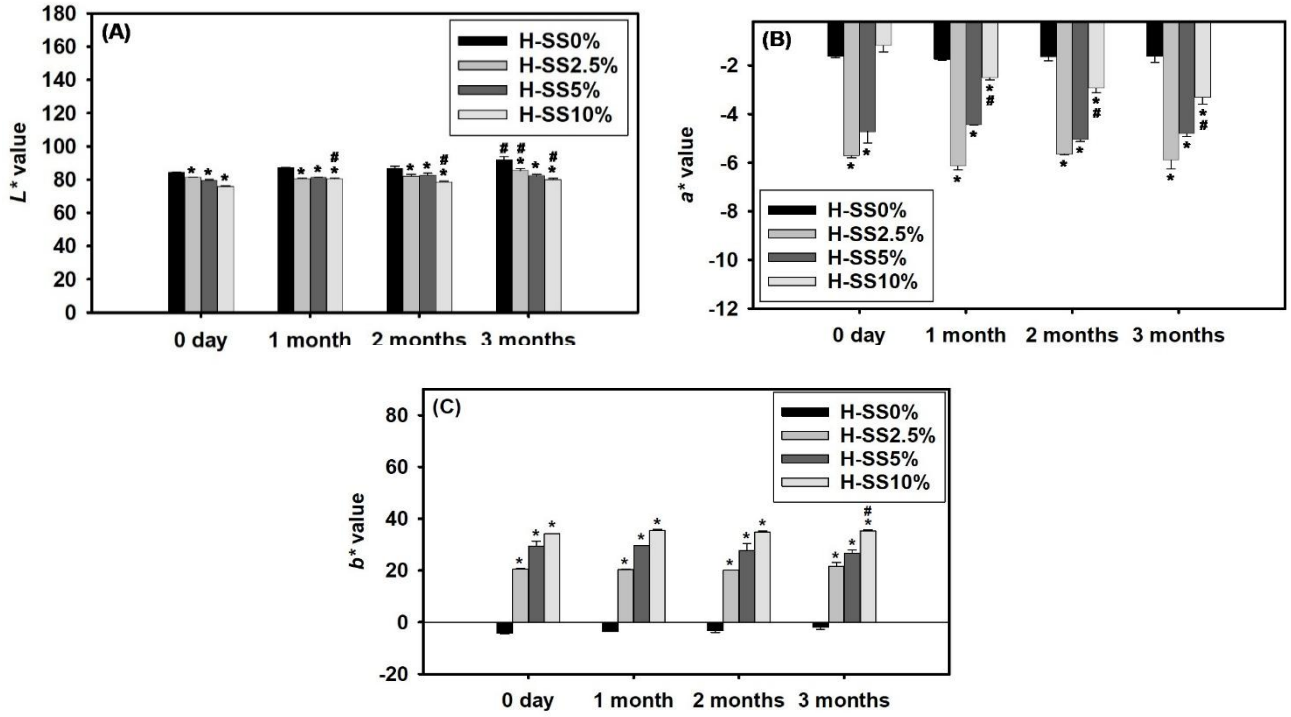

Figure 9 (A) *L**, (B) *a**, and (C) *b** values of color measurement of PVA/CMC/SS hydrogels containing PG extract under storage at 4 °C. $^{*}p < 0.05$ compared with H-SS0% and $^{\#}p < 0.05$ compared with day 0 within the same sample type. Data are expressed as mean ± SD (n = 3).

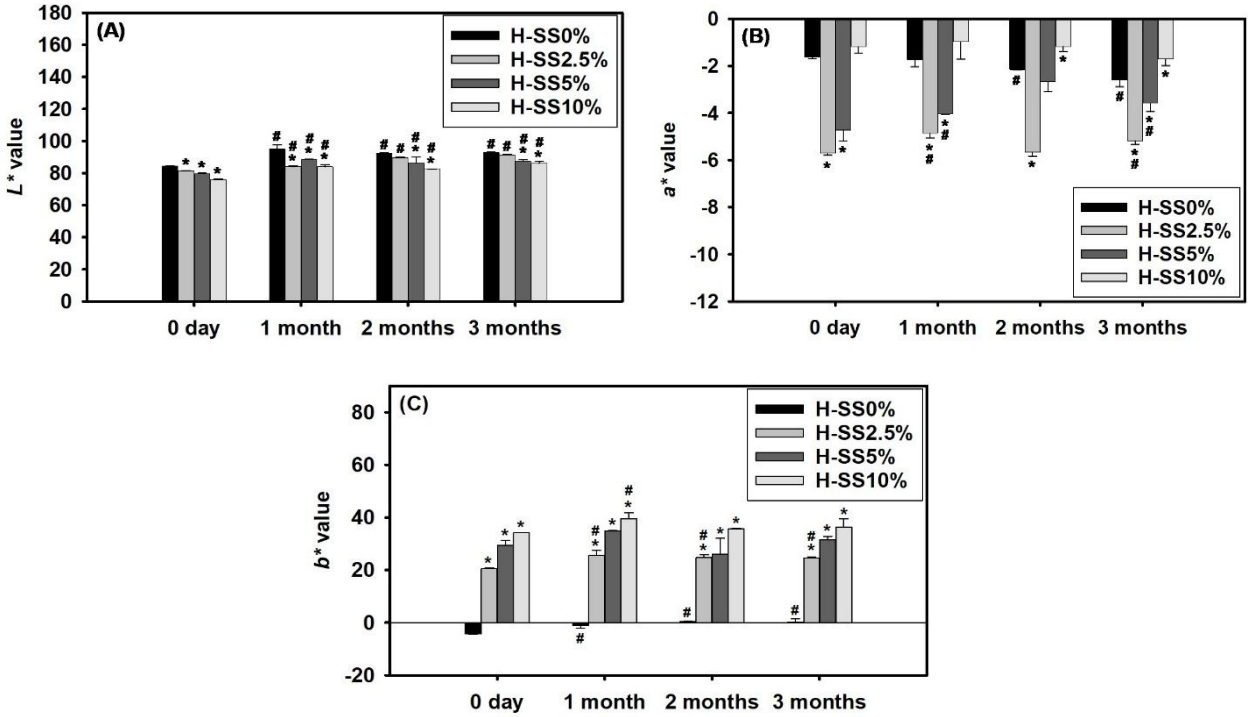

Figure 10 (A) L^*, (B) a^*, and (C) b^* values of color measurement of PVA/CMC/SS hydrogels containing PG extract under storage at 30 °C. $^{*}p < 0.05$ compared with H-SS0% and $^{\#}p < 0.05$ compared with day 0 within the same sample type. Data are expressed as mean ± SD (n = 3).

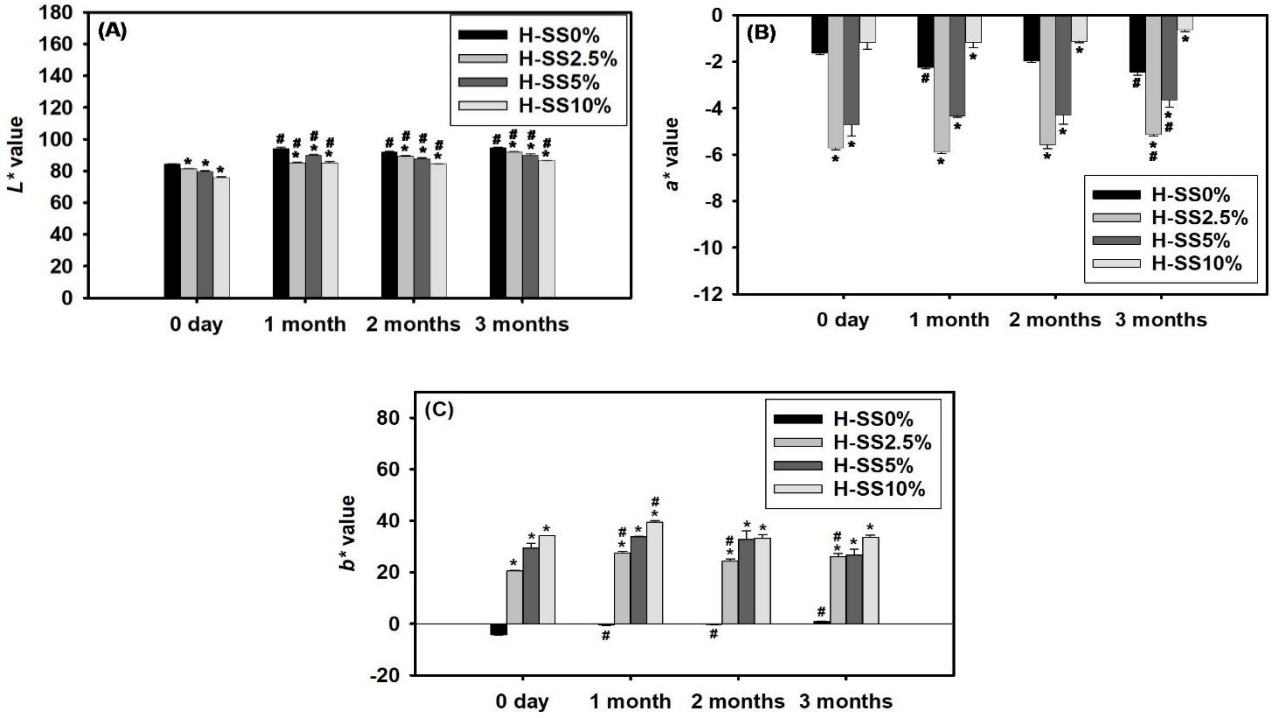

Figure 11 (A) L^*, (B) a^*, and (C) b^* values of color measurement of PVA/CMC/SS hydrogels containing PG extract under storage at 40 °C. $^{*}p < 0.05$ compared with H-SS0% and $^{\#}p < 0.05$ compared with day 0 within the same sample type. Data are expressed as mean ± SD (n = 3).

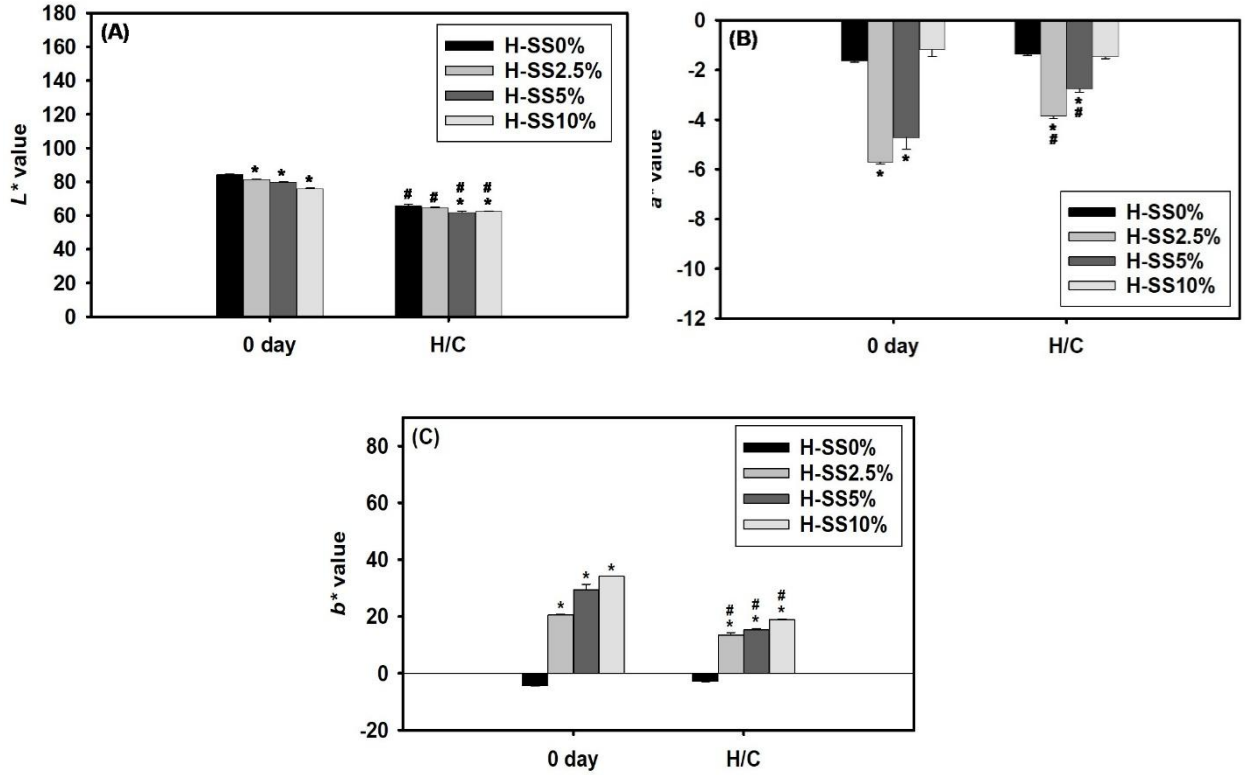

Figure 12 (A) L^*, (B) a^*, and (C) b^* values of color measurement of PVA/CMC/SS hydrogels containing PG extract under storage of H/C cycles. $^{*}p < 0.05$ compared with H-SS0% and $^{\#}p < 0.05$ compared with day 0 within the same sample type. Data are expressed as mean ± SD (n = 3).

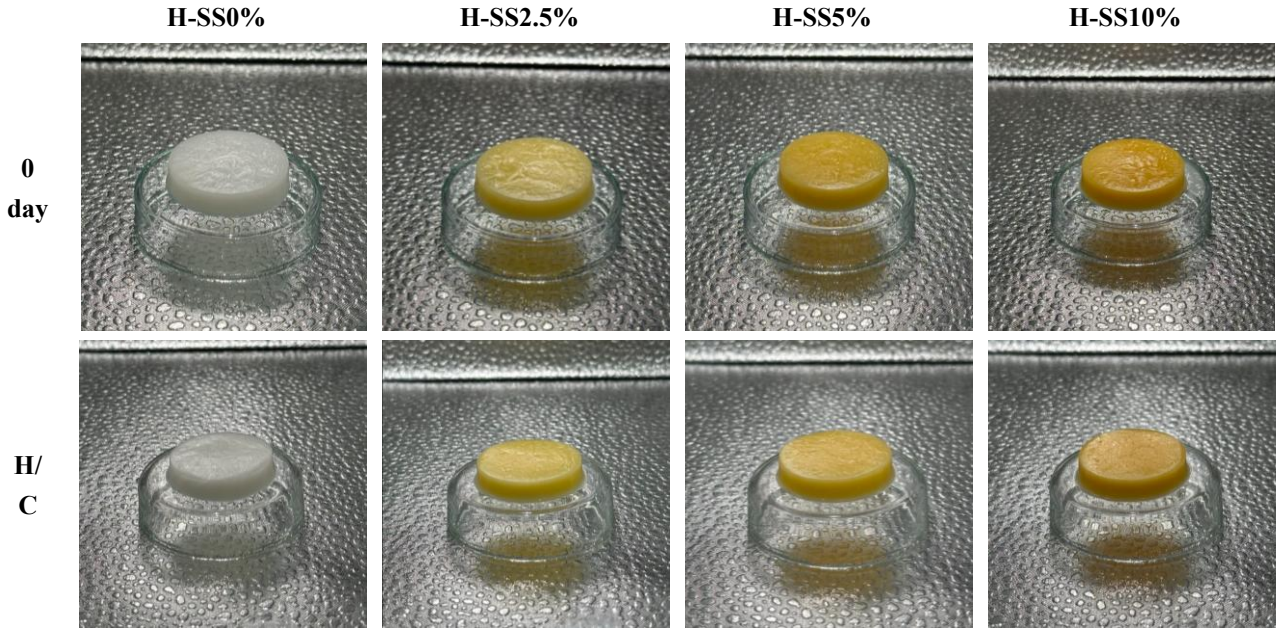

Figure 13 Representative photographs illustrating the physical appearance and color of the PVA/CMC/SS hydrogels containing PG extract before (0 day) and after 7 heating-cooling (H/C) cycles.

Mechanical stability

The mechanical stability of the hydrogels under different storage conditions was evaluated based on compressibility (**Figure 14**) and hardness (**Figure 15**). The compressibility of all formulations increased after 1 month of storage, decreased at 2 months, and

subsequently increased at 3 months. In contrast, the hardness exhibited a different trend, increasing at 1 month and then gradually decreasing over prolonged storage. These results indicate that prolonged storage distinctively alters the network dynamics, affecting its rigidity and work-deformation responses differently. The initial increase in both compressibility and hardness at 1 month may be associated with structural rearrangement within the polymer network, leading to improved packing and intermolecular interactions. However, the subsequent divergence in behavior suggests that prolonged storage affects different aspects of the network [53]. The increase in compressibility at 3 months may be attributed to enhanced chain reorganization, which increases the total work required for deformation. In contrast, the decrease in hardness suggests gradual weakening of the maximum peak force of the network structure, possibly due to the relaxation of polymer chains and a reduction in physical crosslinking density [54,55]. Temperature effects were also evident; hydrogels stored at elevated temperatures (30 and 40 °C) exhibited higher variations in both compressibility and hardness compared to those stored at 4 °C, indicating more pronounced structural modifications under higher temperature conditions. Under heating-cooling (H/C) cycles, both compressibility and hardness increased compared to the initial state. This behavior may be associated with repeated thermally induced rearrangement of polymer chains, which enhances intermolecular interactions and alters mechanical performance [37]. Additionally, these long-term mechanical alterations can be partially attributed to water loss and redistribution during storage and thermal cycling; this dehydration reduces water's natural plasticizing effect, leading to increased stiffness and altered flexibility [56]. In summary, these results demonstrate that storage conditions significantly influence the mechanical behavior of the hydrogels. Refrigerated storage provided more stable mechanical properties, while elevated temperatures and thermal cycling induced noticeable changes in the polymer network structure.

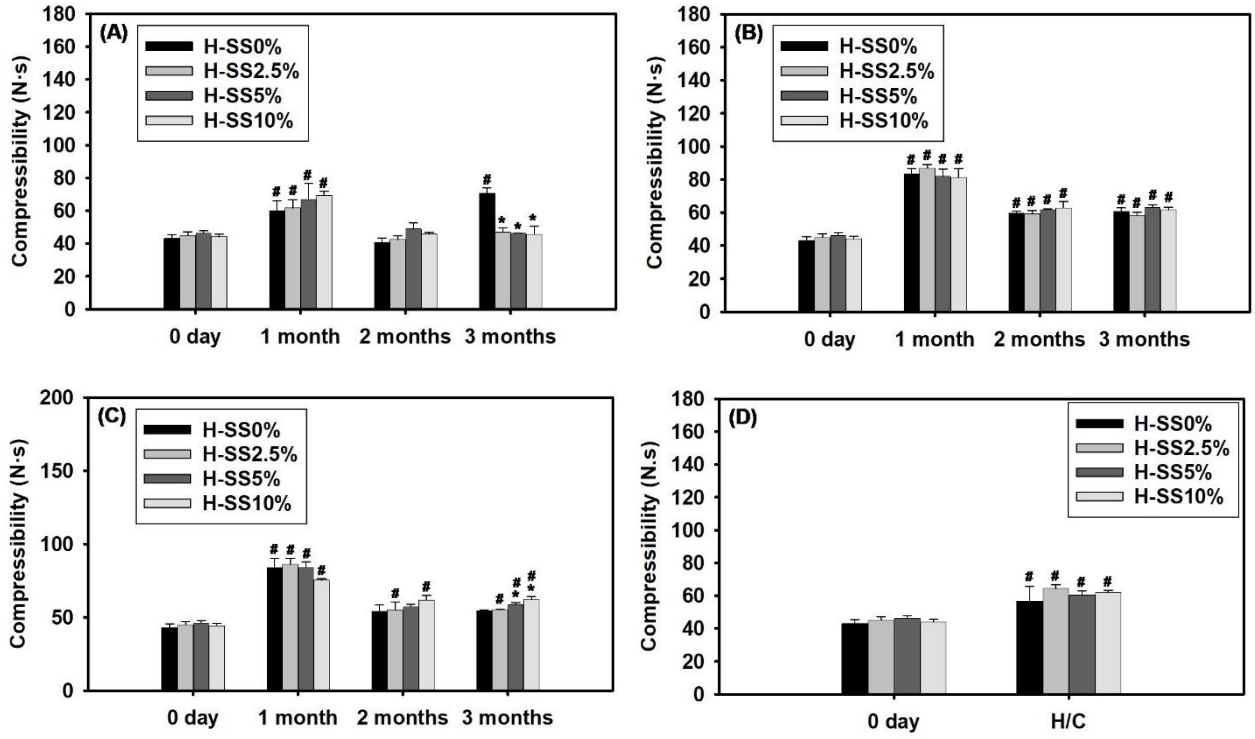

Figure 14 Compressibility of hydrogels under different storage conditions at 4 °C (A), 30 °C (B), 40 °C (C), and H/C (D). $^{*}p < 0.05$ compared with H-SS0% and $^{\#}p < 0.05$ compared with day 0 within the same sample type. Data are expressed as mean ± SD (n = 3).

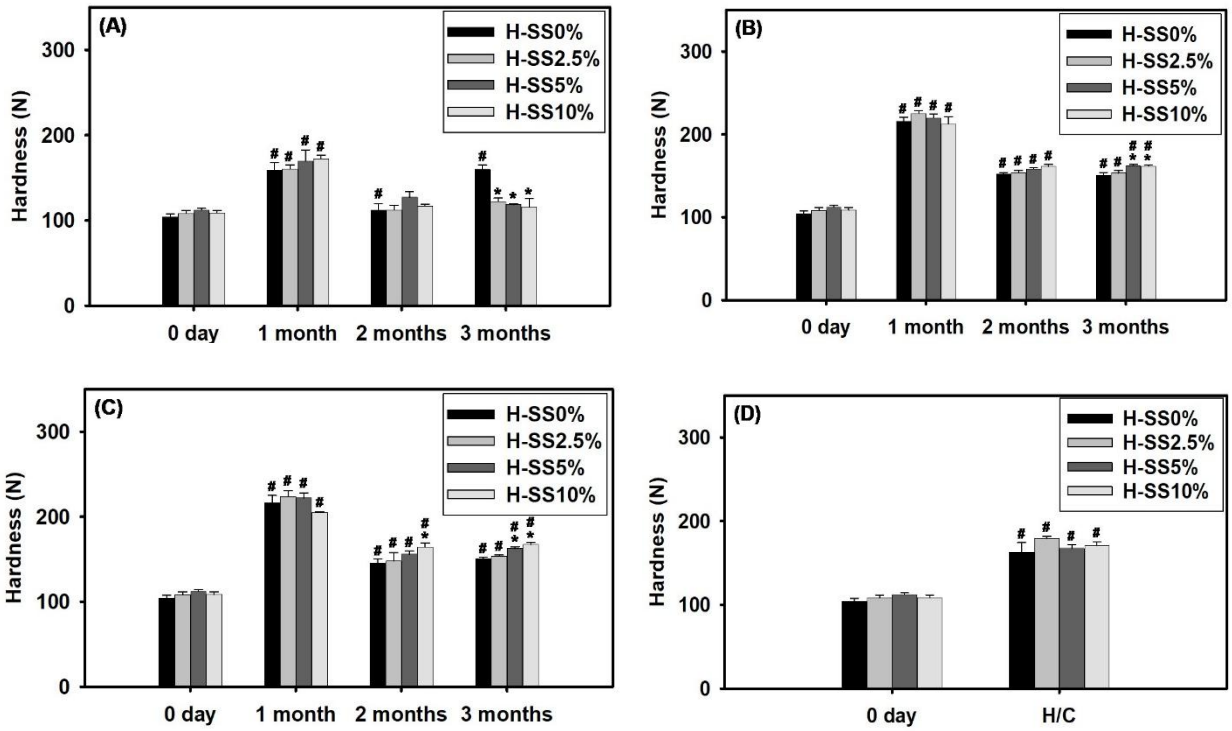

Figure 15 Hardness of hydrogels under different storage conditions at 4 °C (A), 30 °C (B), 40 °C (C), and H/C (D). $^{*}p < 0.05$ compared with H-SS0% and $^{\#}p < 0.05$ compared with day 0 within the same sample type. Data are expressed as mean ± SD (n = 3).

Practical applicability, limitations, and future perspectives

Despite the *in vitro* physicochemical, bioactivity, and preliminary biocompatibility results discussed above, the practical translation of the developed PVA/CMC hydrogels loaded with PG extract and SS into commercial facial masks requires careful consideration of several factors. From a shelf-life perspective, stability studies conducted over a three-month period at 4, 30, and 40 °C, along with alternating heating/cooling cycles, demonstrate the formulation's resilience. The hydrogels, fabricated via a freeze-thaw process, exhibited good structural integrity against thermal fluctuations, with optimal long-term stability observed at lower temperatures (e.g., 4 °C) to mitigate moisture loss and preserve extract bioactivity. However, a notable limitation of the current study is its primary reliance on *in vitro* assessments. Although preliminary cytotoxicity profiles are highly favorable, the absence of human clinical data currently restricts immediate commercial applicability. Therefore, future optimization strategies must prioritize comprehensive *in vivo* safety profiling, including skin sensitization and irritation patch tests, alongside clinical efficacy trials. Additionally, further development should explore specialized packaging to prevent dehydration during prolonged storage, ensuring the long-term commercial viability of these bioactive hydrogels.

Conclusions

The developed PVA/CMC/SS hydrogels containing PG extract demonstrated properties relevant to facial mask applications. PG extract and SS exhibited antioxidant and antityrosinase activities, with IC_{50} values of 0.458% (v/v) and 52.57% (v/v) for PG extract, and 0.337 and 7.19 mg/mL for SS, respectively. The tyrosinase inhibitory activity of the released solution increased with SS addition up to 5%, with no significant difference observed between 5% and 10% SS. Morphological analysis revealed that increasing SS concentration led to a denser, more tightly packed internal network. Despite this structural densification, all formulations maintained an excellent water retention capacity (~87%), ensuring optimal hydration. Furthermore, this compacted structure effectively modulated the biphasic *in vitro* release of the PG extract.

Both the release profile and mechanical analysis indicated that hydrogels containing 5% SS exhibited optimal properties; the H-SS5% formulation successfully minimized the initial burst effect while providing compressibility values of 43 - 46 N·s and hardness values of 104 - 112 N. The adhesive strength increased with SS content, reaching 0.167 kPa at 10% SS. Crucially, indirect cytotoxicity evaluations confirmed the excellent *in vitro* biocompatibility of the hydrogels, maintaining over 80% cell viability in both NCTC clone 929 and HDFa cells for up to 48 h. Colorimetric evaluation showed a slight yellow tint associated with the presence of polyphenolic compounds, while stability studies indicated that storage at 4 °C provided the best preservation of color and mechanical properties. These findings suggest that the developed hydrogels, particularly the H-SS5% formulation, have promising potential as facial mask candidates. However, appropriate storage conditions are required to maintain their physicochemical stability and ensure product performance over time. Furthermore, while *in vitro* biocompatibility was confirmed via cytotoxicity assays, comprehensive clinical evaluations, including human skin irritation and sensitization testing, remain essential in future studies to fully establish their dermatological safety and practical applicability for consumer use.

Acknowledgements

The authors gratefully acknowledge the Scientific and Technological Instruments Center (STIC), Mae Fah Luang University, Thailand for providing laboratory facilities, and the National Nanotechnology Center (NANOTEC) for their support and contributions.

Declaration of Generative AI in Scientific Writing

The authors acknowledge the use of generative AI tools (e.g., Gemini and ChatGPT) in the preparation of this manuscript, specifically for grammar checking, proofreading, improving readability, and language flow. No content generation or data interpretation was performed by AI. The authors take full responsibility for the content and conclusions of this work.

CRediT author statement

Rachata Bunglom: Data curation; Formal analysis; Investigation; Methodology; Writing – original draft. **Porntipa Pankongadisak**: Data curation; Formal analysis; Investigation; Visualization; Writing – original draft. **Kitipong Kiti**: Methodology; Visualization. **Suvimol Surassmo**: Investigation; Validation. **Orawan Suwantong**: Conceptualization; Formal analysis; Methodology; Supervision; Validation; Writing – review & editing

References

[1] Transparency Market Research, Available at: https://www.transparencymarketresearch.com, accessed March 2026.

[2] E Caló and VV Khutoryanskiy. Biomedical applications of hydrogels: A review of patents and commercial products. *European Polymer Journal* 2015; **65**, 252-267.

[3] E Bilgi, EH Gokce, E Bayir, A Sendemir, KO Ozer and EEH Tuna. Bacterial cellulose based facial mask with antioxidant property and high moisturizing capacity. *Cellulose* 2021; **28**, 10399-10414.

[4] H Rao and JBL Tan. Polysaccharide-based hydrogels for atopic dermatitis management: A review. *Carbohydrate Polymers* 2025; **349**, 122966.

[5] W Hu, Z Wang, Y Xiao, S Zhang and J Wang. Advances in crosslinking strategies of biomedical hydrogels. *Biomaterials Science* 2019; **7(3)**, 843-855.

[6] WX Waresindo, HR Luthfianti, A Priyanto, DA Hapidin, D Edikresnha, AH Aimon, T Suciati and Khairurrijal. Freeze–thaw hydrogel fabrication method: Basic principles, synthesis parameters, properties, and biomedical applications. *Materials Research Express* 2023; **10(2)**, 024003.

[7] H Adelnia, R Ensandoost, SS Moonshi, JN Gavgani, EI Vasafi and TH Ta. Freeze/thawed polyvinyl alcohol hydrogels: Present, past and future. *European Polymer Journal* 2022; **164**, 110974.

[8] EA Kamoun, ERS Kenawy and X Chen. A review on polymeric hydrogel membranes for wound dressing applications: PVA-based hydrogel

dressings. *Journal of Advanced Research* 2017; **8(3)**, 217-233.

[9] H Dai, Y Huang and H Huang. Eco-friendly polyvinyl alcohol/carboxymethyl cellulose hydrogels reinforced with graphene oxide and bentonite for enhanced adsorption of methylene blue. *Carbohydrate Polymers* 2018; **185**, 1-11.

[10] V Tyagi and A Thakur. Carboxymethyl cellulose-polyvinyl alcohol based materials: A review. *Materials Today: Proceedings* 2023. https://doi.org/10.1016/j.matpr.2023.01.042

[11] Y Sun, F Shi, R Tian, X Zhao, Q Li, C Song, Y Du, X He and J Fu. Fabrication of versatile polyvinyl alcohol and carboxymethyl cellulose-based hydrogels for information hiding and flexible sensors: Heat-induced adjustable stiffness and transparency. *International Journal of Biological Macromolecules* 2023; **253(3)**, 126950.

[12] AAP Mansur, MA Rodrigues, NSV Capanema, SM Carvalho, DA Gomes and HS Mansur. Functionalized bioadhesion-enhanced carboxymethyl cellulose/polyvinyl alcohol hybrid hydrogels for chronic wound dressing applications. *RSC Advances* 2023; **13(19)**, 13156-13168.

[13] V Sethi, M Kaur, A Thakur, P Rishi and A Kaushik. Unravelling the role of hemp straw derived cellulose in CMC/PVA hydrogel for sustained release of fluoroquinolone antibiotic. *International Journal of Biological Macromolecules* 2022; **222**, 844-855.

[14] JK Liu. Natural products in cosmetics. *Natural Products and Bioprospecting* 2022, **12**, 40.

[15] S Gilotra, D Chouhan, N Bhardwaj, SK Nandi and BB Mandal. Potential of silk sericin based nanofibrous mats for wound dressing applications. *Materials Science and Engineering: C* 2018; **90**, 420-432.

[16] M Saad, LM El-Samad, RA Gomaa, M Augustyniak and MA Hassan. A comprehensive review of recent advances in silk sericin: Extraction approaches, structure, biochemical characterization, and biomedical applications. *International Journal of Biological Macromolecules* 2023; **250**, 126067.

[17] S Mohanty, A Mishra, N Gupta, B Varunteja, T Mukherjee, P Pradhan, A Kumari, N Nayak, A Sahu, PK Prabhakar and MA Ansari. Sericin as a next-generation biomaterial: Properties, applications, and future prospects. *International Journal of Biological Macromolecules* 2025; **319(2)**, 145393.

[18] HR Rahimi, M Arastoo and SN Ostad. A comprehensive review of *Punica granatum* (Pomegranate) properties in toxicological, pharmacological, cellular and molecular biology researches. *Iranian Journal of Pharmaceutical Research* 2012; **11(2)**, 385-400.

[19] JH Ruan, J Li, G Adili, GY Sun, M Abuduaini, R Abdulla, M Maiwulanjiang and HA Aisa. Phenolic compounds and bioactivities from pomegranate (*Punica granatum* L.) peels. *Journal of Agricultural and Food Chemistry* 2022; **70(12)**, 3678-3686.

[20] J Du, H Wang, L Zhong, S Wei, X Min, H Deng, X Zhang, M Zhong and Y Huang. Bioactivity and biomedical applications of pomegranate peel extract: A comprehensive review. *Frontiers in Pharmacology* 2025; **16**, 1569141.

[21] Y Tumbarski, I Ivanov, R Vrancheva, N Mazova and K Nikolova. Pomegranate peels: A promising source of biologically active compounds with potential application in cosmetic products. *Cosmetics* 2025; **12(4)**, 169.

[22] EM Akl, MS Hasanin and S Dacrory. Skin mask hydrogel-based natural sources: Characterization and biological properties evaluations. *Bioactive Carbohydrates and Dietary Fibre* 2023; **29**, 100355.

[23] M Shi, S Wu, M Xie, R Xiong, A Yang and C Huang. A biocompatible anti-aging gel mask prepared with sappanwood extract and sodium carboxymethyl cellulose, exhibiting antioxidant and antibacterial properties. *International Journal of Biological Macromolecules* 2025; **322(1)**, 146588.

[24] D Puspitasari, AM Anwar, DSG Ananda, G Reza, A Jusuf and LATW Asri. Porous Sericin/PVA/Moringa oleifera hydrogels: Physical properties and hyperelastic model. *Procedia Structural Integrity* 2024; **52**, 410-417.

[25] LM El-Samad, MA Hassan, AA Basha, S El-Ashram, EH Radwan, KKA Aziz, TM Tamer, M Augustyniak and AE Wakil. Carboxymethyl

cellulose/sericin-based hydrogels with intrinsic antibacterial, antioxidant, and anti-inflammatory properties promote re-epithelization of diabetic wounds in rats. *International Journal of Pharmaceutics* 2022; **629**, 122328.

[26] F Jokar, S Rahaiee, M Zare, MN Kenari and N Mirzakhani. Bioactive wound dressing using bacterial cellulose/dextran biopolymers loaded with pomegranate peel extract: Preparation, characterization and biological properties. *Journal of Drug Delivery Science and Technology* 2023; **84**, 104461.

[27] DF Ferreira, TM da Silva, RCG de Melo, KA Bastos, JGM Ucella-Filho, JA Severi, JCO Villanova and JA Resende. Development of a gel formulation with pomegranate peel extract (*Punica granatum* L.) for antimicrobial and wound healing action. *South African Journal of Botany* 2024; **173**, 284-294.

[28] A Kaolaor, K Kiti, P Pankongadisak and O Suwantong. *Camellia oleifera* oil-loaded chitosan nanoparticles embedded in hydrogels as cosmeceutical products with improved biological properties and sustained drug release. *International Journal of Biological Macromolecules* 2024; **275(1)**, 133560.

[29] XC Bo, DC Wang, YX Liu and MH Li. Degradable cellulose/polylactic acid facial masks with antibacterial and antioxidant action from pomegranate extract. *Cellulose* 2023; **30**, 6959-6970.

[30] P Pankongadisak and O Suwantong. The potential use of thermosensitive chitosan/silk sericin hydrogels loaded with longan seed extract for bone tissue engineering. *RSC Advances* 2018; **8(70)**, 40219-40231.

[31] P Pankongadisak, K Kiti, J Yang, L Grøndahl and O Suwantong. Multifunctional injectable self-healing hydrogels based on quaternized chitosan-gallic acid and oxidized pectin for use in wound management. *International Journal of Biological Macromolecules* 2026; **348**, 150746.

[32] OA Fawole, NP Makunga and UL Opara. Antibacterial, antioxidant and tyrosinase-inhibition activities of pomegranate fruit peel methanolic extract. *BMC Complementary and Alternative Medicine* 2012; **12**, 200.

[33] X Cao, X Ding, R Chen, Y Li, A Tehoungue, W Huang, G Kang, G Zhang and Y Zhang. Explore the antioxidative and tyrosinase inhibitory activity of green sericin resources from different fibroin-deficient silkworm varieties. *Journal of Food Measurement and Characterization* 2025; **19**, 593-602.

[34] S Napavichayanun, W Bonani, Y Yang, A Motta and P Aramwit. Fibroin and polyvinyl alcohol hydrogel wound dressing containing silk sericin prepared using high-pressure carbon dioxide. *Advances in Wound Care* 2019; **8(9)**, 452-462.

[35] E Mitani, Y Ozaki and H Sato. Two types of C=O···HO hydrogen bonds and OH···OH (dimer, trimer, oligomer) hydrogen bonds in PVA with 88% saponification/PMMA and PVA with 99% saponification/PMMA blends and their thermal behavior studied by infrared spectroscopy. *Polymer* 2022; **246**, 124725.

[36] M Yooyod, GM Ross, N Limpeanchob, N Suphrom, S Mahasaranon and S Ross. Investigation of silk sericin conformational structure for fabrication into porous scaffolds with poly(vinyl alcohol) for skin tissue reconstruction. *European Polymer Journal* 2016; **81**, 43-52.

[37] CM Hassan and NA Peppas. *Structure and applications of poly(vinyl alcohol) hydrogels produced by conventional crosslinking or by freezing/thawing methods*. Springer, Germany, 2000, p. 37-65.

[38] T Siritientong, J Ratanavaraporn, T Srichana and P Aramwit. Preliminary characterization of genipin-cross-linked silk sericin/poly(vinyl alcohol) films as two-dimensional wound dressings for the healing of superficial wounds. *BioMed Research International* 2013; **2013**, 904314.

[39] NA Dahlan, J Pushpamalar, AK Veeramachineni and S Muniyandy. Smart hydrogel of carboxymethyl cellulose grafted carboxymethyl polyvinyl alcohol and properties studied for future material applications. *Journal of Polymers and the Environment* 2018; **26**, 2061-2071.

[40] L Ricci, E Umiltà, MC Righetti, T Messina, C Zurlini, A Montanari, S Bronco and M Bertoldo. On the thermal behavior of protein isolated from different legumes investigated by DSC and TGA.

Journal of the Science of Food and Agriculture 2018; **98(14)**, 5368-5377.

[41] Q He, D Huang, J Yang, Y Huang and S Wang. Dual cross-link networks to preserve physical interactions induced by soaking methods: Developing a strong and biocompatible protein-based hydrogel. *ACS Applied Bio Materials* 2019; **2(8)**, 3352-3361.

[42] D Kundu, A Jayaraman and CK Sen. Clinical measurement of transepidermal water loss. *Advances in Wound Care* 2026; **15(2)**, 73-90.

[43] R Fatahian, A Fatahian, E Fatahian and H Fatahian. A critical review on application of silk sericin and its mechanical properties in various industries. *Journal of Research and Applications in Mechanical Engineering* 2021; **9(2)**, 1-11.

[44] HY Wang, HD Wang and YQ Zhang. A mechanically robust PVA-xylosylated sericin composite hydrogel membrane with enhanced biocompatibility by unidirectional dehydration through nanopore. *Polymer Testing* 2023; **124**, 108062.

[45] M Shitole, S Dugam, R Tade and S Nangare. Pharmaceutical applications of silk sericin. *Annales Pharmaceutiques Françaises* 2020; **78(6)**, 469-486.

[46] I Duggal, AN Martinez, NR Richbourg and NA Peppas. Network theory and recent developments in networks formed by the freeze–thawing process. *Polymer* 2026; **344**, 129385.

[47] H Xue, J Feng, Y Tang, X Wang, J Tang, X Cai and H Zhong. Research progress on the interaction of the polyphenol–protein–polysaccharide ternary systems. *Chemical and Biological Technologies in Agriculture* 2024; **11**, 95.

[48] CC Lin and AT Metters. Hydrogels in controlled release formulations: Network design and mathematical modeling. *Advanced Drug Delivery Reviews* 2006; **58(12-13)**, 1379-1408.

[49] WHD Jong, JW Carraway and RE Geertsma. *In vivo and in vitro testing for the biological safety evaluation of biomaterials and medical devices*. *In*: JP Boutrand (Ed.). Biocompatibility and performance of medical devices. 2nd ed. Woodhead Publishing, Cambridge, 2020, p. 123-166.

[50] S Ferreyra, R Bottini and A Fontana. Temperature and light conditions affect stability of phenolic compounds of stored grape cane extracts. *Food Chemistry* 2023; **405**, 134718.

[51] S Pandit, S Kumar, D Ganguly, P Sardar, S Nandi, M Mandal, S Chattopadhyay, A Roy, D Pradhan and RK Das. Freeze–thaw-induced, metal ion cross-linked, mechanically robust, and highly stretchable composite poly(vinyl alcohol) hydrogels for flexible electronic applications. *ACS Applied Polymer Materials* 2024; **6(13)**, 7631-7647.

[52] JL Holloway, AM Lowman and GR Palmese. The role of crystallization and phase separation in the formation of physically cross-linked PVA hydrogels. *Soft Matter* 2013; **9(3)**, 826-833.

[53] YN Jo, BD Park and IC Um. Effect of storage and drying temperature on the gelation behavior and structural characteristics of sericin. *International Journal of Biological Macromolecules* 2015; **81**, 936-941.

[54] MGA Vieira, MA da Silva, LO dos Santos and MM Beppu. Natural-based plasticizers and biopolymer films: A review. *European Polymer Journal* 2011; **47(3)**, 254-263.

[55] H Levine and L Slade. *Water as a plasticizer: Physico-chemical aspects of low-moisture polymeric systems*. Cambridge University Press, Cambridge, 1988, p. 79-185.

[56] NE Suyatma, L Tighzert, A Copinet and V Coma. Effects of hydrophilic plasticizers on mechanical, thermal, and surface properties of chitosan films. *Journal of Agricultural and Food Chemistry* 2005; **53(10)**, 3950-3957.